Journal of Materials Chemistry A

Accepted Manuscript

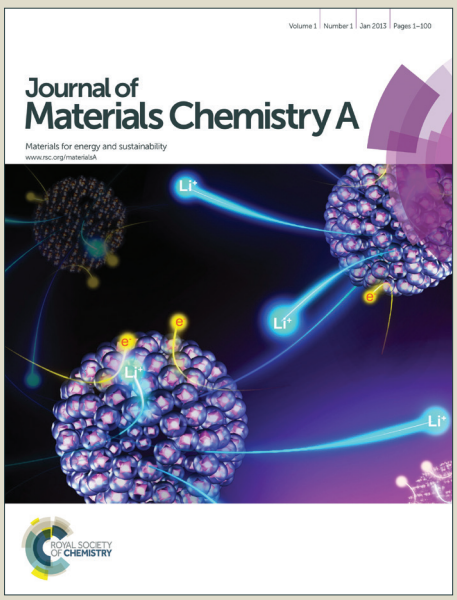

ROYAL SOCIETY OF CHEMISTRY

www.rsc.org/materialsA

Journal of Materials Chemistry A

ARTICLE

Structural investigation of co-evaporated methyl ammonium lead halide perovskite films during growth and thermal decomposition using different PbX_2 (X=I,Cl) precursors

Received 00th January 20xx,
Accepted 00th January 20xx

DOI: 10.1039/x0xx00000x

www.rsc.org/

Juliane Borchert,[a] Heidi Boht,[a] Wolfgang Fränzel,[a] René Csuk,[a] Roland Scheer [a,*] and Paul Pistor[a,*,+]

Abstract While the progress in device development of perovskite solar cells is rapidly evolving, details of the film formation and the interplay of processing parameters, structural and compositional properties of deposited phases and their stability are still under dispute. Here we present a detailed structural analysis of methylammonium lead halide (I,Cl) films by *in situ* X-ray diffraction during their growth and thermal recrystallization up to their decomposition. $MAPbI_3$ films grown by coevaporating MAI and PbI_2 are compared to $MAPbI_3(Cl)$ films derived from an evaporation route using MAI and $PbCl_2$ precursors. The main differences observed between the two routes are varying crystal structures at room temperature and differently limited process windows, but similar overall growth, recrystallization and decomposition features. The preferential orientation of the pure $MAPbI_3$ is shown to depend on the applied molar precursor flux ratio and can additionally be modified by thermal annealing.

Introduction

Hybride organic-inorganic perovskite materials have been studied for some decades because of their unique optical and electronic properties and the huge opportunities they offer to tailor properties by combining organic and inorganic components.[1,2] But it was the successful application of lead halide perovskites as absorber material in photovoltaic devices that has boosted interest and research in the last few years.[3-5]
The development of perovskite solar cells has undergone a tremendously fast progress leading to devices already surpassing 20% power conversion efficiencies.[6] These high efficiencies have been mainly achieved on the basis of methylammonium (MA) lead halide perovskite, where the halide generally is iodide ($MAPbI_3$)[7-10] or a mixture of iodide and chloride ($MAPb(I,Cl)_3$)[11-13].
There is a lot of effort put in the development of this new class of solar cell materials. This resulted in the development of a variety of deposition methods[7,12-15] device architectures[16-20] and variations of the absorber constituents,[21-23] all leading to high efficiency devices. This multitude of successful approaches stresses the flexibility and intrinsic potential as light harvester of this impressive material. A good review on the recent fast advances of perovskite solar cells can be found in reference 5.
Most preparation approaches have been based on solution processing of the absorber films, but there are also several promising reports on the deposition of very uniform films with large crystal grains by co-evaporation.[24-27] This makes co-evaporation especially attractive for the preparation of planar solar cells, enabling an easily scalable deposition of high quality films under very controlled conditions, with a broad choice of precursors available for an easy variation of composition or even doping of the absorber material.
Recently, the monitoring of phase formation with *in situ* X-ray diffraction (XRD) during the growth of $MAPb(I,Cl)_3$ perovskites by co-evaporation of methylammonium iodine (MAI) and $PbCl_2$ has been reported.[27] In this contribution, we will compare the growth of $MAPb(I,Cl)_3$ with different precursor flux ratios (MAI, PbI_2 and $PbCl_2$). We will show how a change of the precursor from $PbCl_2$ to PbI_2 affects the structure and growth of the perovskite films. In addition, the effect of different molar flux ratios of the organic and the inorganic precursor on the film texture will be analysed. For this we will use a detailed structure analysis by X-ray diffraction and will in the following shortly review the crystal structure of $MAPb(I,Cl)_3$.
There are several theoretical as well as experimental studies on the crystal structure of the organometal halide perovskites.[28-31] The general perovskite structure is based on a cubic unit cell consisting of five atoms with chemical formula ABX_3, where the cation B is surrounded by 6 nearest neighbour anions X, and the cation A by twelve. For the methylammonium lead halides ($A=CH_3NH_3$, B=Pb, X=I,Cl,Br), the O_h symmetry of this cubic perovskite structure is preserved in the higher temperature α-phase (space group *Pm3m*), where the non-centrosymmetric organic MA molecules are randomly oriented.[32] The transition temperature $T_{\alpha-\beta}$, where the structure transforms into a tetragonal β-phase (space group *I4/mcm*) decreases from $MaPbI_3$ (+57°C) to $MAPbBr_3$

[a] Martin-Luther-Universität Halle-Wittenberg, Halle (Saale), Germany
* Corresponding author: roland.scheer@physik.uni-halle.de, ppistor@irec.cat
† Current address: IREC – Catalonia Insitute for Energy Research, Sant Adria de Besos – Barcelona, Spain

(−36.9°C) to $MAPbCl_3$ (−96.0°C). At even lower temperatures, the methyl ammonium lead halides crystallise in an orthorhombic structure with space group *Pbnm*. A very comprehensive description of the crystal phases, transitions and XRD patterns of $MAPbI_3$ powder material was given by Baiki et al.[33]

Different preferential grain orientations for polycrystalline thin films have been reported in literature depending on the varying deposition conditions. The crystallographic texture hasbeen reported to dependent on the applied solvents,[34] the ratio of the applied precursors in the case of solution-processed solar cells and are more pronounced for $MAPbI_3(Cl)$ films derivated from Cl-based precursors films than for films involving only I-based precursors.[35,36]

While the achievable extremely high open circuit voltages, the band gap tuneability, the ease and low-cost fabrication processes involved and the astonishing power conversion efficiencies raise lots of enthusiasm for perovskite solar cells, the toxicity of the heavy metal Pb as well as the stability of devices and the perovskite material itself have raised some concern.

The ease of intercalation of MAI into the PbI_2 host structure has the advantage of enabling fast preparations at low temperatures (down to room temperature). But on the other hand, this ease of intercalation seems to come along without a likewise easy liberation, and an intrinsically limited stability of the material. There have been numerous reports on the degradation and/or decomposition of perovskite-based devices under the influence of moisture, oxygen or UV-light.[37-39] Moisture and ambient air condition have been clearly identified to trigger the decomposition of hybrid lead halide perovskites into MAI and PbI_2 if not properly sealed.[40] Thermal stress is also known to cause the decomposition of these materials, whereas the temperature where this decomposition starts is discussed controversially as outlined below.

On the other hand, a mild thermal annealing is generally needed for high performance of devices processed at low temperatures.[41] This thermal treatment is expected to remove residual solvents and enhance the crystallisation and optoelectronic properties of the perovskite thin film. A detailed analysis of the thermal behaviour is therefore of special interest for a variety of reasons. Dualeh[41] et al. presented a detailed thermogravimetric analysis of solution processed $MAPbI_3(Cl)$ films lately, where they found that at temperatures above 300°C the organic component of the perovskite decomposes by the subsequent loss of HI and CH_3NH_2. Tan[41] et al. found in an in situ grazing incidence XRD study that thermal annealing of solution-processed $MAPb(I,Cl)_3$ films for 50 min. at 100°C induced only minor decomposition to PbI_2 if applied in an nitrogen atmosphere, but strong PbI_2 contributions were observed if the treatment was carried out in ambient air. Supasai[42] et al. detected PbI_2 by a change in the surface photovoltage and XRD signature after an annealing at 140°C.

In this contribution, the effect of a thermal treatment will be studied in detail and *in situ* by an careful XRD analysis in order to investigate its impact on the recrystallisation, phase transitions and decomposition of co-evaporated perovskite $MAPbI_3$ and $MAPbI_3(Cl)$ thin films under vacuum conditions.

The working temperature of a solar cell depends on the climatic conditions, ventilation and insolation, but can easily surpass 60ºC in unfavourable conditions. For the most commonly used absorber compound $MAPbI_3$, this would imply repeated transitions between the α- and β-phase ($T_{\alpha-\beta}$ = 57ºC) which might possibly deteriorate the device performance in the long term. This is another reason why detailed structure analysis and characterization as targeted in this work might turn out to be an important tool in the investigations of the degradation and decomposition of these absorbers.

In our current contribution we therefore first compare the formation of $MAPbI_3$ perovskite thin films grown by MAI and PbI_2 precursors to $MAPbI_3(Cl)$ films grown from MAI and $PbCl_2$ precursors. The influence of the molar flux ratios on the film texture and the formation of secondary phases will be investigated in a second step. Finally a careful analysis of the structural changes will elucidate recrystallisation and decomposition effects induced by heating of the thin films.

Experimental

All experiments were performed in a vacuum chamber, which is exclusively used for the physical vapour deposition of perovskite thin films. The base pressure in the vacuum chamber is < 10^{-5} mbar before starting the evaporation. Multiple effusion cells are used to evaporate the MAI, PbI_2 and $PbCl_2$ precursors. During the process various techniques are used to monitor the film growth, namely a laser light scattering system (LLS), several thermocouples, a quartz microbalance (QMB) and an in situ X-ray diffraction (XRD) setup. The setup was modelled after a chamber used for the growth of kesterite and chalcopyrite thin films. For details on the measurement setup, the interested reader is referred to references 27 and 43.

The XRD measurements are performed using a Cu X-ray source and a detector array which is capable of measuring a 2θ diffraction angle range of 28° simultaneously. In order to enable reasonably short acquisition times, during the *in situ* measurements the incident angle is kept fixed at 12.5° and the detector array is placed to cover the 2θ diffraction angle range from 11° to 38° simultaneously in one measurement. During the measurements presented here, a diffractogram was taken every 30s. We call this measurement geometry a 2θ-scan in contrast to the commonly used θ/2θ-scan in Bragg-Brentano geometry in which both the incident angle and diffracted angle are varied. The arrangement with fixed incidence angle makes mechanical movements of the detector/source unnecessary and enables time-resolved observations of the phases in the growing film. Compositional and structural changes can be observed and analyzed this way. *In situ* XRD provides information about the crystal phases already during the growth of the film and can be used as process monitoring, making adjustments during the process possible.

The substrates are mounted on a heatable substrate holder placed above the evaporation sources. During a typical growth

process the substrate was actively cooled and kept at a temperature around 15°C. To monitor the temperature of the sample, for example during annealing, a thermocouple is placed in contact with the back of the substrate. A quartz microbalance (QMB) is placed next to the substrate to monitor the growth rate of the film. Tooling factors for the microbalance were determined by analysing the LLS signals to estimate the film thickness and were verified using mechanical profilometer measurements. Methylammonium iodide (MAI) was synthesized in the group of Prof. Csuk. Lead iodide and lead chloride were purchased from Alfa Aesar and possessed purities of 99.9985% and 99.999% respectively. During standard depositions MAI was heated to temperatures between 110 and 120°C, $PbI_2$to between 210 and 240°C and the $PbCl_2$ precoursor to temperatures between 340°C and 370°C.

During thin film growth, material is not only deposited on the substrate, but also on the kapton foils through which the X-rays enter and exit the chamber. The covering layers on the kapton windows absorb part of the X-ray light reducing the X-ray intensity reaching the detector. To reduce the influence of this effect, the windows are replaced after each deposition run. In the presentation of the evolution of peak heights presented in Figure 1 b), a correction was applied to account for this increasing absorption: Prior to and after each run the intensity of the X-ray beam is measured as it exits the chamber. We observed that during a typical growth process, the intensity decreases by around 20%. Assuming a linear growth of the absorbing covering layers, these intensities were used to estimate the exponential damping of the X-rays at each moment of the deposition process and the peak intensity evolution was corrected accordingly.

The molar fluxes of PbX_2 and MAI were determined using two distinct approaches. The PbI_2 and $PbCl_2$ fluxes were determined from the overall growth rate under the assumption that all of the lead reaching the substrate sticks to the substrate and is incorporated into a stoichiometric perovskite film. The overall mass increase on the substrate is measured by the QMB. In order to obtain the PbX_2 mass flux rate, the overall mass flux rate is multiplied by the mass fraction that PbX_2 accounts for in the stoichimetric perovskite. The mass fraction is obtained by dividing the molecular mass of PbX_2 by the molecular mass of $MaPbI_3$. The obtained mass flux rate for PbX_2 is converted into a molar flux using the molar masses of PbI_2 (461g/mol) and $PbCl_2$ (276g/mol). It is known that not all of the offered MAI is incorporated into the film during growth and that the MAI rate can often not be properly detected using a QMB.[26,27] The molar flux of MAI was therefore estimated from the chamber pressure during evaporation. The ideal gas law and the Maxwell-Boltzmann speed distribution were utilized for these calculations. This approach gives a low estimate of the MAI flux, as the concentration of MAI at the pressure sensor may be lower than at the substrate, which is placed in a straight line above the source.

For the standard growth experiments we used a substrate temperature of ~15°C during the complete deposition period. The MAI molar fluxes were fixed providing chamber pressures of 5×10^{-5}mbar (MAI-PbI_2 evaporation) and 2.5×10^{-4}mbar (MAI-PbI_2 evaporation), PbX_2 fluxes were kept at 2.5×10^{-11} mol/cm^{2}s (PbI_2) and 7×10^{-11} mol/cm^{2}s ($PbCl_2$). In EDX measurements we find a halide/(halide+Pb) ratio in the perovskite films grown under these conditions of 0.75 or above as would be expected if the PbI_2 has been intercalated with sufficient MAI to form the perovskite film. The resulting growth rates were 0.4 Å/s (PbI_2) and 1.1Å/s ($PbCl_2$) and the final film thickness in both cases were ~450 nm.

The XRD diffractograms obtained during the *in situ* measurements were analysed using the Rigaku Data Analysis Software PDXL2. Split pseudo-Voigt functions were used to fit the reflexes of each diffractogram to extract peak positions, heights, areas and full widths at half maximum (FWHM) values. Symmetry and decay rate factors are kept constant for each peak to increase the accuracy and comparability of the automatic fit. Peaks are identified using literature values[33] and the Powder Diffraction File Database PDF-4+..

Results and Discussion

$MAPb(I,Cl)_3$ growth by co-evaporation of MAI and PbI_2 or $PbCl_2$

As outlined above, many highest efficient perovskite solar cells are derived from $PbCl_2$-based precursors, leading to improved diffusion lengths and device properties.[36,45] The application of $PbCl_2$-based precursors is believed to enhance the crystal growth. Unlike the $MAPb(I,Br)_3$ system, there is no solid solution between the Iodine-based $MAPbI_3$ and the $MAPbCl_3$ and even for perovskite films grown from $PbCl_2$ precursors the amount of Cl incorporated into the finished films is rather low. The actual amount of Cl incorporated into the film is debated controversially and seems to depend on the applied deposition method. However, it is clear that the amount of Cl in the halide content is rather low, generally reported to be below 5% and the perovskite films derived from $PbCl_2$ precursor resemble $MAPbI_3$ films in their optical and structural properties.[27,35,46] Throughout this work, we will therefore refer to these films as $MAPbI_3$(Cl). However, the structural implications of the chloride addition still remain unclear and pend further investigations. Here, we compare the growth of thin films using either lead chloride ($PbCl_2$) or lead iodide (PbI_2), co-evaporated with methyl ammonium iodide (MAI). During these experiments the evaporation parameters (source temperatures, substrate temperature) are kept constant over the complete deposition period.

Figure 1 shows panels of XRD reflex intensities, full width at half maximum (FWHM), and 2θ peak positions of $MAPbI_3$ films grown from PbI_2+MAI (left) and of $MAPbI_3$(Cl) growth from MAI+$PbCl_2$ (right). Using both types of precursors, the XRD patterns can be indexed by the perovskite structure according to reference 33. As discussed in a previous publication[27] films grown under these conditions with MAI and $PbCl_2$ precursors contain approximately 2% chloride in the halide component, with the remaining 98% of halide being iodide. As expected,

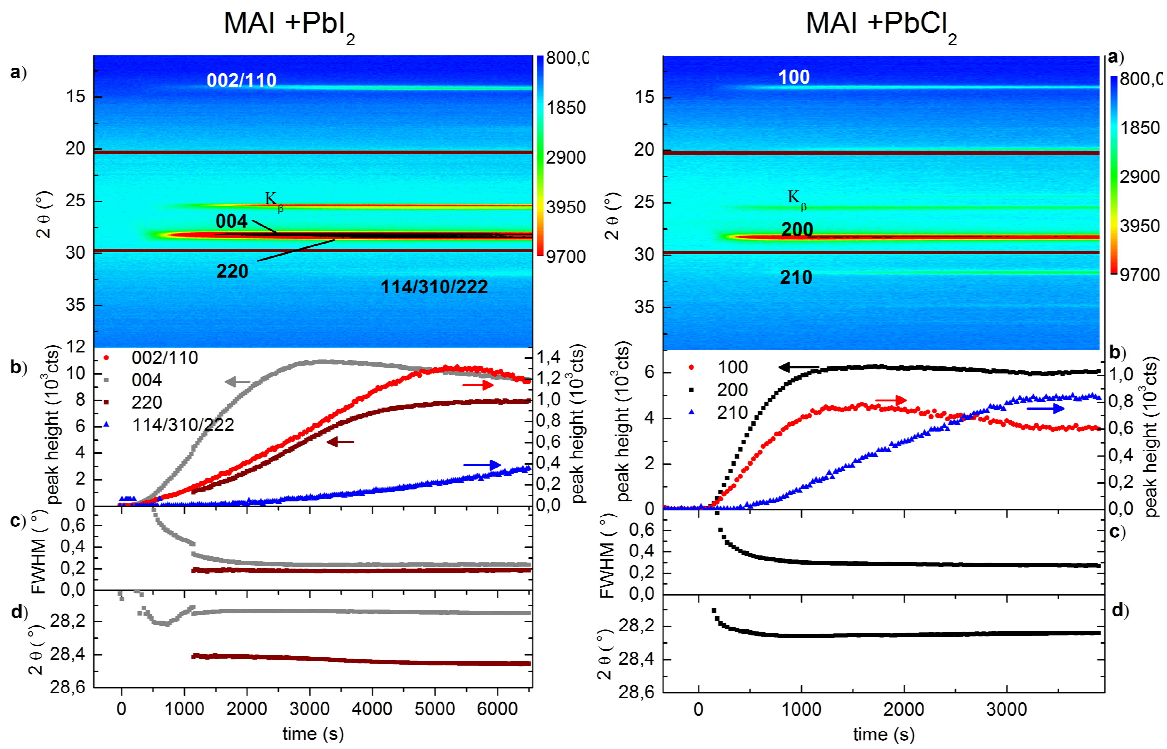

Fig. 1 Growth processes using MAI as well as PbI_2 (left) or $PbCl_2$ (right) as precursors. (a) Color maps of X-ray diffraction with intensity scales and peak labels. Reflexes of $MAPbI_3$ (left) are indexed with a tetragonal symmetry (β-phase), reflexes of $MAPbI_3$(Cl) (right) are indexed according to the cubic α-structure. K_β marks the positions of the reflexes of the 004/220 and 200 peaks stemming from the K_β-excitation line. (b) Peak heights for main perovskite reflexes. (c) FWHM and (d) 2θ angle values of 004 and 220 (left) as well as of 200 (right) reflexes.

films grown with MAI and PbI_2 do not contain any chloride according to energy dispersive X-ray spectroscopy (EDX). The dynamics of the film growth can be seen in **Figure 1** (b-d) where time *t*= 0s marks the opening of the PbX_2 shutter.The MAI flux was initiated at time *t*= - 2000s.

For both lead precursos, PbI_2 and $PbCl_2$, approximately 300s after opening of the PbX_2 shutters the first XRD reflexes appear and as the films grow, the peak heights rise and simultaneously the FWHM decreases. Using the Debye-Scherrer formula, the FWHM can be translated into a crystal size. In the initial growth phase, this crystal size is equal to the film thickness; therefore we estimate a 3-dimensional growth regime.

After approximately 1000s, the FWHM stays nearly constant and a slight decrease of the 100 and 200 peak height is observed, while the 210 peak increases. This indicates that the 100/200 orientation initially is preferred, but as the film thickness increases crystallites with a 210 orientation grow as well. This happens in a similar manner both, for films grown with $PbCl_2$ and with PbI_2. The final films exhibit similar textures with 100 and 200 peaks dominating in the conclusive θ-2θ scan for the $MAPbI_3$, and 002/110 and 004/220 peaks for the $MAPbI_3$(Cl). This preferential orientation is in agreement with the findings of other authors.[35,36,47] We note that due to the 2θ-geometry, texture here means that a certain lattice vector is *nearly* normal to the surface.

An important difference between the two growth processes is the observed splitting of several reflexes when PbI_2 is used. The cubic 100 reflex observed in the $MAPbI_3$(Cl) splits into the tetragonal 002 and 110 reflexes, the 200 reflex splits into the 004 and 220 and at the approximate position of the cubic 210 reflex the three 114, 310 and 222 are observed in the tetragonal structure.[27,33]

To show this difference more clearly, details of the XRD patterns recorded at the end of the deposition processes with and without Cl are compared in **Figure 2 a)**. For the $MAPbI_3$ sample a peak splitting is seen, which is not observed for the chloride containing sample. $MAPbI_3$ is known to crystallize in a tetragonal structure at room temperature with a transition to the cubic structure around 57°C.[31] In the following experiments we observed this transition during the annealing of the samples. Hence, we can clearly index the observed split peaks at 2θ=28.13° and 28.45° as the 004 and 220 reflexes of the tetragonal structure with space group *I4/mcm* for this $MAPbI_3$ film. Other $MAPbI_3$ films showed only a single reflex, however always matching the peak position of either one of the tetragonal reflexes. An example is shown in **Figure 2 b)** for a $MAPbI_3$ film labelled "strong texture" exhibiting a single reflex at around 2θ=28.14°. This film has a strong orientation favouring 004. It has been grown with a 1.7-fold higher PbI_2 flux at an identical MAI flux. This suggests that a high PbI_2 flux may lead to a strong 004 orientation, but, there may be other factors influencing the growth of the 004 orientation over 220 orientation. We will show how the different precursor fluxes influence the grain orientation in more detail in the next section.

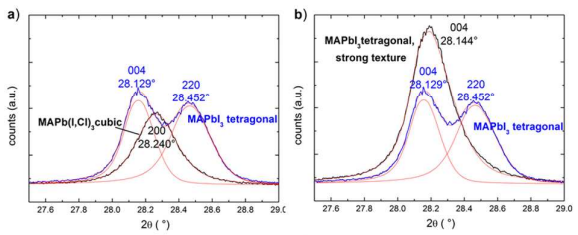

Figure 2 (a) Details of single diffractograms from the growth of $MAPbI_3(Cl)$ and $MAPbI_3$ films extracted from the end of the growth processes depicted in Figure 1. (b) Comparison of two $MAPbI_3$ growth experiments with different grades ofpreferential orientation of the grains (texture) as a result of different PbI_2 fluxes.

As previously reported by Pistor et al., co-evaporated films grown with $PbCl_2$ precursors under similar conditions finally contained only around 2% Cl in the halide component and showed diffraction patterns which matched better the cubic than to the tetragonal perovskite structure. Figure 2 now proves that for $MAPbI_3(Cl)$, not only the reflex splitting is missing but the observed reflex is also not at the 2θ position of either tetragonal reflex. Hence, the assignment of the cubic crystal structure with space group *Pm3m* to films containing only 2% Cl of the halide component is correct.

To summarize, we found that both PbI_2 and $PbCl_2$ can be used to grow metal-organic halide $MAPb(I,Cl)_3$ perovskite films with the co-evaporation method. The films are clearly differentiated by their crystal structure at room temperature. Films grown using PbI_2 and MAI possess a tetragonal structure, whereas films grown with $PbCl_2$ and MAI are in the cubic phase at room temperature. Because of the possibility of a strongly oriented tetragonal phase, with only one visible reflex instead of the characteristic split peak, great care needs to be taken when crystal structures are assigned, based on single, un-split XRD reflexes. Whether a grown film is in the tetragonal or cubic phase might be of importance in stability considerations, because films in tetragonal configuration are prone to undergo repeated structural transitions under operating conditions.

Growth with different evaporation rates

The precursor flux is one of the growth parameters which can be changed relatively easily during a physical vapour deposition. Therefore it is desirable to know how the fluxes can be used to control the grown thin film phases. Earlier it was found that when MAI and $PbCl_2$ are used as precursors, a small $PbCl_2$ flux leads to a chloride poor $MAPbI_3$-derived phase (phase A, $MAPbI_3(Cl)$ while a large $PbCl_2$ flux leads to a chloride rich phase, which we called phase B and which crystal structure features resembled the ones of $MAPbCl_3$. [27] Phase B contains roughly 50% chloride in the halide part and is nearly optically transparent. Here, we show how changes in the MAI to PbI_2 flux rates affect the $MAPbI_3$ growth and compare them with the $MAPbI_3(Cl)$ growth in order to assess the limiting fluxes of secondary phase formation. For these experiments the MAI crucible temperature was kept constant, while the PbX_2 crucible temperature was linearly increased from 180°C to 340°C (PbI_2) and from 350°C to 465°C ($PbCl_2$). The molar flux ratio was determined as described in the Experimental section. In **Figure 3 a)** we see the integrated reflex intensities for co-evaporation of MAI and PbI_2 for different molar flux ratios. At small molar flux ratios, the most prominent reflex is the tetragonal 220 reflex at 28.4°. Only as the rate increases, the 004 reflex at 28.1° appears and later becomes dominant. The texture of the $MAPbI_3$ film appears to depend on the PbI_2 precursor flux. Very low fluxes result in a 220 orientation, mid to high fluxes lead to increased 004 growth. This is in agreement with Figure 2 where a large 004 peak was induced by a higher PbI_2 flux.

At slightly higher PbI_2 fluxes, additional reflexes at 23° and 35.5° appear, which can be matched to PbI_2 and I, respectively. This indicates that for high PbI_2 fluxes, lead iodide and iodide are deposited as secondary phases directly onto the substrate. We compare this result with a MAI-$PbCl_2$ co-evaporation ramp depicted in **Figure 3 b)**. There, the formation of $PbCl_2$ secondary phases takes place at much higher molar MAI/$PbCl_2$ flux ratios and is accompanied by a steep decline of the $MAPbI_3(Cl)$ intensities. In reference 27 it was shown that at

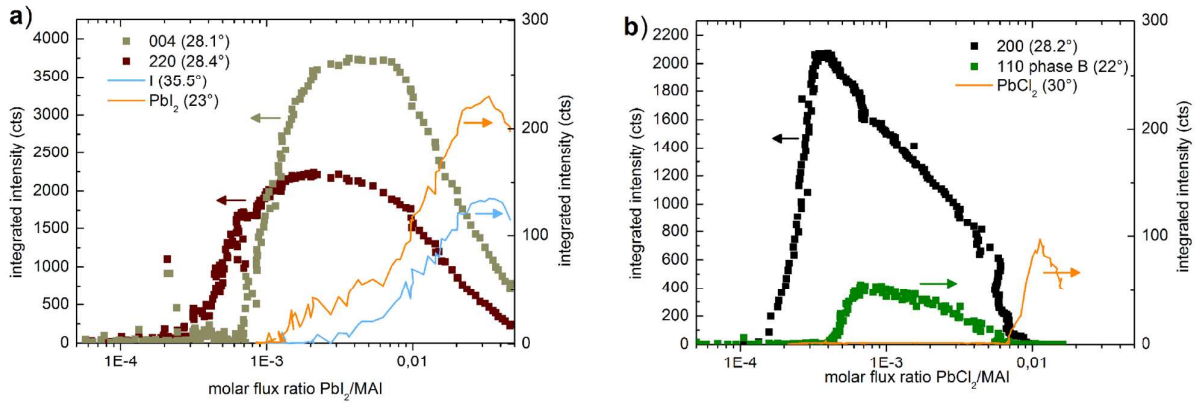

Fig. 3 Integrated peak intensities during the co-evaporation of a) MAI-PbI_2 and b) MAI-$PbCl_2$ under increasing molar flux ratios. The increase of the flux ratios was accomplished within 100 minutes by linearly ramping the PbX_2 temperature at constant MAI flux. Final film thicknesses are 7 µm and 10 µm for MAI-PbI_2 and MAI-$PbCl_2$ coevaporation, respectively.

high $PbCl_2$ fluxes corresponding to a crucible temperature of 400°C and just before the onset of the growth of $PbCl_2$ secondary phases, there is a growth regime where no XRD peaks are observed under constant film formation (detected by the laser interference maxima). This indicates the growth of an amorphous film for the co-evaporation of MAI and $PbCl_2$. No similar growth regime is found for MAI-PbI_2 coevaporation. While the process window for the growth of the $MAPbI_3$(Cl) phase A under MAI-$PbCl_2$ co-evaporation is determined by the onset of the formation of phase B (high Cl), the process window for $MAPbI_3$ derived from MAI-PbI_2 coevaporation is limited by the formation of a PbI_2 secondary phase.

In conclusion we found that the flux of PbX_2 strongly influences which phases grow, both for depositions with PbI_2 and with $PbCl_2$. With increasing PbI_2/MAI molar flux ratios the 004 orientation begins to dominate over the 220 orientation. For even higher flux ratios, PbI_2 is formed which limits the process window for the growth of single phase $MAPbI_3$. For evaporations using $PbCl_2$ as precursor, higher $PbCl_2$/MAI flux ratios result in the growth of a chloride rich phase with film properties which are undesirable for solar cells. This similarly limits the process window for the growth of $MAPbI_3$(Cl) absorber layers.

Annealing of the $MAPbI_3$ and $MAPbI_3$(Cl) thin films

Thermal treatment is a field of interest, because on one hand, many researchers have used post deposition annealing in the fabrication of solar cells with high efficiencies.[13,24,48] On the other hand, sensitivity to elevated temperatures is considered to be one factor contributing to the instability of perovskite solar cells.[49] To investigate the phase changes during thermal treatment of perovskite films, the grown films were heated on a linear ramp from 15°C to 350°C in 100 min. in vacuum (no MAI flux). Over the entire period, XRD measurements took place. The development of the reflex heights during the heating is shown for both a chloride free (a) and chloride containing (b) film in **Figure 4**.

For the chloride containing $MAPbI_3$(Cl) film in Fig. b), the perovskite's 100, 200, and 210 peaks slightly increase up to about 150°C and then show a pronounced growth upon ramping from 150°C to 200°C. Also the FWHM exhibits a remarkable decrease down to below 0.1° after passing 150°C and reaches a minimum value of FWHM=0.057°. (Note that the instrumental peak width of our XRD system is 0.05°.) Both, the increased peak intensities and decreased FWHM indicate a recrystallization of the chloride containing film, during which the crystallite size is increased and the 200 texture is enhanced. This observation is consistent with the fact that in the fabrication of highly efficient perovskite solar cells, annealing steps are found to be beneficial.[13,24,48] Above 200°C the heights of the perovskite reflexes decline rapidly, the FWHM increases, and PbI_2 and Pb reflexes appear. This evidences a decomposition of the perovskite material. While our XRD technique probes effectively the bulk, the decomposition is expected to occur first at the film surface as was reported earlier.[50] Above 250°C the XRD reflexes corresponding to the perovskite structure completely disappeared. Above 300°C the PbI_2 reflexes also decrease and disappear. Finally, above 320 °C only a small reflex attributed to metal Pb remains. Dualeh[41] et al. showed that the decomposition of films grown from PbI_2 and $PbCl_2$ precursors proceeds by a loss of the organic perovskite component upon annealing under atmospheric nitrogen pressure. The methyl ammonium undergoes dissociation where first HI is desorbed and then CH_3NH_2 is sublimed. The desorption temperature was found to be 300°C for a Cl containing film and 350°C for the pure $MAPbI_3$. The fact that these authors found higher decomposition temperatures could be due to the difference in the pressure under which the experiments were performed as well as differences in the preparation methodology leading to

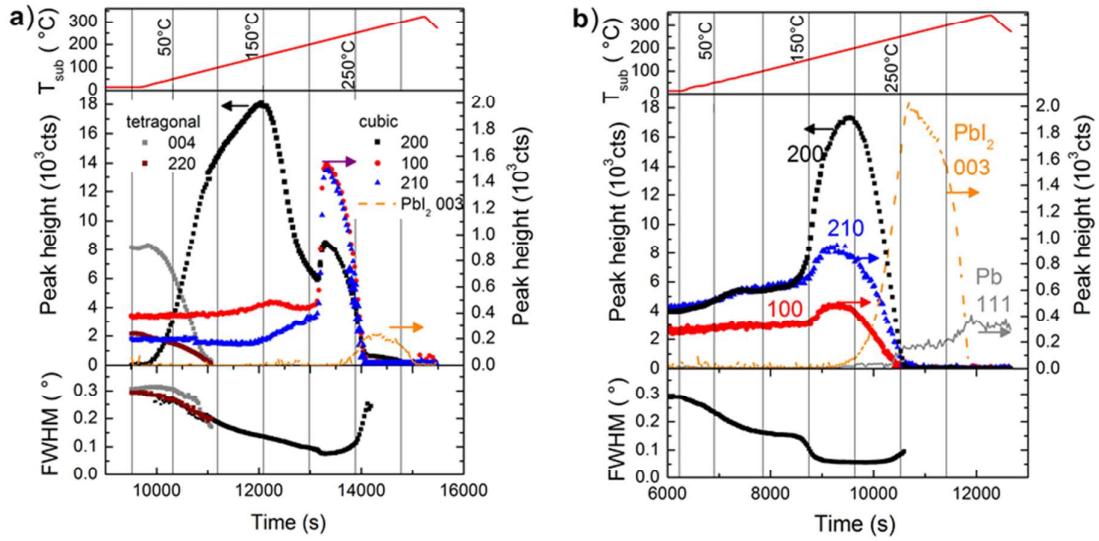

Fig. 4 Peak intensity of selected reflexes over time during the heating of a $MAPbI_3$ film (a) and a $MAPbI_3$(Cl) film (b). Vertical lines indicate the temperature every 50°C. Below the development of the FWHM of selected reflexes is shown.

differences in film density.

The pure $MAPbI_3$ film prepared from the PbI_2 precursors is tetragonal at room temperature (see also Figure 2), evidenced by splitting of the characteristic peaks (e.g. 004/200). As the sample is heated, the 004 and 220 reflexes decrease in height and a new reflex appears. The position of this reflex is in-between the 004/220 split peaks and matches that of the 200 reflex of the cubic perovskite phase indicating the transition to the cubic α-phase at temperatures around 50°C. After transition, the height of the 200 reflex further increases at the same time as the FWHM decreases from 0.25° to 0.14°. This again indicates the improvement of the crystallinity of the film. At approximately 150°C the reflex height starts to drop significantly and rises again at temperatures slightly above 200°C. Above 250°C new reflexes matching PbI_2 appear. Finally, above 300°C these also decrease until no reflexes are left. The final drop of the perovskite reflexes and the appearance of new reflexes, indicate the decomposition of the perovskite. The earlier temporary drop between 150°C and 250°C cannot be explained by a decomposition, as subsequently reflex height increases again between 200°C and 250°C, the FWHM keeps decreasing and no additional reflexes were observed. This behaviour was repeatedly observed for films prepared on glass substrates and cannot be explained to full extent at present, but is assumed to be related to texturing effects caused by changing preferential orientations of the film. This is supported by the fact that films grown on Mo-coated glass substrates, which differed in their primary film orientation, did not show this double maximum for the 200 peaks.

In summary, for both, chloride-free and chloride-containing films, first a recrystallization and then decomposition into PbI_2 is observed. The films which contain only iodide, show additionally a transition from the tetragonal to the cubic phase at around 50°C. When comparing films grown from the two precursors, we observe first evidences of decomposition at slightly lower temperatures for the $PbCl_2$-precursor route. Both perovskite films are completely decomposed at temperatures around 250°C.

In situ monitoring of phase changes and decomposition occurring during thermal treatment is suggested to assess and compare the stability of various other metalorganic halide perovskites in future experiments.

Conclusions

In this contribution, we showed how the analysis of XRD patterns recorded in situ during the growth and thermal annealing of methyl ammonium lead halide thin films allows to distinguish different phases and preferential orientations of the absorber material and allows to assess the formation of secondary phases and the decomposition of the material at elevated temperatures. We compared $MAPb(I,Cl)_3$ thin films derived from the evaporation of MAI and PbI_2 or $PbCl_2$ in detail and found similarities as well as significant differences: While pure $MAPbI_3$ films as derived from MAI and PbI_2 evaporation crystallised as expected in the tetragonal β-phase at room temperature and underwent the reported $\beta-\alpha$ transition at temperatures around 50°C, we confirmed the $MAPbI_3(Cl)$ films deposited by the evaporation of MAI and $PbCl_2$ to be cubic already at room temperature. The phase formation is largely governed by the ratio of the MAI to PbX_2 flux. In the case of $MAPbI_3$, the process window for single phase $MAPbI_3$ phase formation is limited by the appearance of PbI_2 secondary phases. Additionally, the MAI to PbI_2 flux ratio was found to significantly influence the orientation of the deposited films. In contrast to this, the process window for $MAPbI_3(Cl)$ deposition was limited by the appearance of a different, transparent and Cl-rich $MAPb(I,Cl)_3$ perovskite phase. During thermal annealing, a recrystallization with increasing XRD intensities and decreasing FWHMs was observed for both films, before they completely decomposed into PbI_2 for temperatures above 250°C and finally to metallic Pb. The start of the decomposition was observed at slightly lower temperatures for the $MAPbI_3(Cl)$ sample. At lower temperatures up to 230°C, the pure $MAPbI_3$ sample showed additional changes in the preferred orientation upon annealing, with a repeatedly observed double maximum in peak height evolution, which also has been tentatively attributed to ongoing orientational changes in the sample.

These detailed structural investigations are expected to deepen the general understanding of absorber film growth as well as structure and temperature related stability issues and by this help the further progress in the development of perovskite applications such as solar cells.

Acknowledgements

Partly funding by the European Union under grant no. GA 625840 ("JumpKEST") is gratefully acknowledged.

References

1 R.E. Wasylishen, O. Knop, J.B. Macdonald, *Solid State Communications*, 1985, **56** (7), 581-582.
2 Mitzi, D. B. in *Progress in Inorganic Chemistry*. Wiley-Blackwell, 1999; Chapter Synthesis, Structure, and Properties of Organic-Inorganic Perovskites and Related Materials, Vol. 48, 1-121.
3 H.J. Snaith, *The Journal of Physical Chemistry Letters* 2013**, 4** (21), 3623-3630.
4 H.S. Kim, S. Im, N.-G. Park, *The Journal of Physical Chemistry C* 2014, **118** (11), 5615-5625.
5 S. Brittman, G.W.P Adhyaksa, E.C. Garnett, *MRC* 2015, **5** (1), 7-26.
6 M.A. Green, K. Emery, Y. Hishikawa, W. Warta, E.D. Dunlop, *Prog. Photovolt: Res. Appl.* 2014, **23** (1), 1-9.
7 J. Burschka, N. Pellet, S.-J. Moon, R. Humphry-Baker, P. Gao, M.K. Nazeeruddin, M. Grätzel, *Nature* 2013, **499** (7458), 316-319.
8 D. Liu, T.L. Kelly, *Nature Photonics* 2014**, *8*,** 133-138.
9 F. Huang, Y. Dkhissi, W. Huang, M. Xiao, I. Benesperi, S. Rubanov, Y. Zhu, X. Lin, L. Jiang, Y. Zhou, A. Gray-Wealeb, J. Etheridge, C.R. McNeill, R.A. Caruso, U. Bach, L. Spiccia, Y.-B. Cheng, *Nano Energy*, 2014, **10**, 10-18

10 W. Ke, G. Fang, J. Wang, P. Qin, H. Tao, H. Lei, Q. Liu, X. Dai, X. Zhao, *ACS Applied Materials & Interfaces,* 2014, **6**, 15959-15965.
11 J.M. Ball, M.M. Lee, A. Hey, H.J. Snaith, *Energy & Environmental Science* 2013, **6** (6), 1739.
12 C.-W. Chen, H.-W. Kang, S.-Y. Hsiao, P.-F. Yang, K.-M. Chiang, H.-W. Lin, Advanced Materials, 2014, **26**, 6647–6652
13 H. Zhou, Q. Chen, G. Li, S. Luo, T.-B. Song, H.-S. Duan, Z. Hong, J. You, Y. Liu, Y. Yang, *Science*, 2014, **345**, 542-546
14 M.J. Carnie, C. Charbonneau, M.L. Davies, J. Troughton, T.M. Watson, K. Wojciechowski, H. Snaith, D. Worsley, *Chemical Communications*, 2013, **49**, 7893
15 L.K. Ono, S. Wang, Y. Kato, S.R. Raga, Y. Qi, *Energy Environ. Sci.*, 2014, **7**, 3989-3993
16 B. Conings, L. Baeten, C. De Dobbelaere, J. D´Haen, J. Manca, H.-G. Boyen, *Advanced Materials* 2014, **26**, 2041-2046
17 S. Aharon, B.-E. Cohen, L. Etgar, *The Journal of Physical Chemistry C*, 2014, **118**, 17160–17165
18 J.H. Heo, S.H. Im, *physica status solidi (RRL) - Rapid Research Letters* 2014, **8**, 816-821
19 P. Docampo, J. Ball, M. Darwich, G.E. Eperon, H.J. Snaith, *Nature Communcations*, 2013, **4**, 2761
20 J.-Y. Jeng, Y.-F. Chiang, M.-H. Lee, S.-R. Peng, T.-F. Guo, P. Chen, T.-C. Wen, *Advanced Materials* 2013, **25** (27), 3727-3732
21 N. Pellet, P. Gao, G. Gregori, T.-Y. Yang, M.K. Nazeeruddin, J. Maier, M. Grätzel, *Angewandte Chemie International Edition*, 2014, **53**, 3151
22 H. Choi, J. Jeong, H.-B. Kim, S. Kim, B. Walker, G.-H. Kim, J.Y. Kim, *Nano Energy*, 2014, **7**, 80-85
23 M. Yang, R. Guo, K. Kadel, Y. Liu, K. O´Shea, R. Bone, X. Wang, J. He, W. Li, *Journal of Material Chemistry A*, 2014, **2**, 19616-19622
24 M. Liu, M.B. Johnston, H.J. Snaith, *Nature*, 2013, **501,** 395-3998
25 O. Malinkiewicz, A. Yella, Y.H. Lee, G. Minguez Espallargas, M. Graetzel, M.K. Nazeeruddin, H.J. Bolink, *Nature Photonics*, 2014, **8**, 128-132
26 L.E. Polander, P. Pahner, M. Schwarze, M. Saalfrank, C. Koerner, K. Leo, *APL Materials*, 2014, **2**, 081503
27 P. Pistor, J. Borchert, W. Fränzel, R. Csuk, R. Scheer, *Journal of Physical Chemistry Letters*, 2014, **5**, 3308-3312
28 A. Poglitsch, D. Weber, *The Journal of Chemical Physics*, 1987, **87**, 6373
29 H. Mashiyama, M. Kurihara, *Journal of the Korean Physical Society*, 1998, **32,** S156-S158
30 Y. Kawamura, H. Mashiyama, *Journal of the Korean Physical Society*, 1999, **35,** 1437
31 Y. Kawamura, H. Mashiyama, K. Hasebe, *Journal of the Physical Society of Japan*, 2002, **71,** 1694-1697
32 W. Yin, J. Yang, J. Kang, Y. Yan, S.-H. Wei, *Journal of Materials Chemistry A*, 2015, **3**, 8926-8942
33 T. Baiki, Y. Fang, J. Kadro, M. Schreyer, F. Wei, S.G. Mhaisalkar, M. Graetzel, T.J. White, *J. Mater. Chem. A*, 2013, **1**, 5628
34 J. Lian, Q. Wang, Y. Yuan, Y. Shao, J. Huang, *Journal of Materials Chemistry A*, 2015, **3**, 9146
35 E.L. Unger, A.R. Bowring, C.J. Tassone, V.L. Pool, A. Gold-Parker, R. Cheacharoen, K.H. Stone, E.T. Hoke, M.F. Toney, M.D. McGehee, *Chemistry of Materials*, 2014, **26**, 7158-7165
36 E. Edri, S. Kirmayer, A. Henning, S. Mukhopadhyay, K. Gartsman, Y. Rosenwaks, G. Hodes, D. Cahen, *Nano Letters*, 2014, **14**, 1000-1004
37 J.H. Noh, S.H. Im, J.H. Heo, T.N. Mandal und S.I. Seok, *Nano Lett.*, 2013, **13**, 1764-1769
38 T. Leijtens, G.E. Eperon, S. Pathak, A. Abate, M.M. Lee, H.J. Snaith, *Nature Communications*, 2013, **4**, 2885
39 G. Niu, W. Li, F. Meng, L. Wang, H. Dong, Y. Qiu, *Journal of Materials Chemistry A*, 2013, **2**, 705
40 S.N. Habisreutinger, T. Leijtens, G.E. Eperon, S.D. Stranks, R.J. Nicholas, H.J. Snaith, *Nano Letters*, 2014, **14**, 5561-5568
41 A. Dualeh, P. Gao, S.I. Seok, M.K. Nazeeruddin, and M. Grätzel, *Chemistry of Materials*, 2014, **26**, 6160-6164
42 K.W. Tan, D.T. Moore, M. Saliba, H. Sai, L.A. Estroff, T. Hanrath, H.J. Snaith, U. Wiesner, *ACS Nano*, 2014, **8**, 4730-4739
43 T. Supasai, N. Rujisamphan, K. Ullrich, A. Chemseddine, T. Dittrich, *Applied Physics Letters*, 2013, **103**, 183906
44 G. Kaune, S. Hartnauer, R. Scheer, *physica status solidi (a)* **2014,** *211,* 1991-1996
45 S.D. Stranks, G.E. Eperon, G. Grancini, C. Menelaou, M.J.P. Alcocer, T. Leijtens, L.M. Herz, A. Petrozza, H.J. Snaith, *Science,* 2013*,* **342**, 341-344.
46 S. Colella, E. Mosconi, P. Fedeli, A. Listorti, F. Gazza, F. Orlandi, P. Ferro, T. Besagni, A. Rizzo, G. Calestani, G. Gigli, F. De Angelis, R. Mosca *Chemistry of Materials,* 2013, **25**, 4613-4618.
47 H. Yu, F. Wang, F. Xie, W. Li, J. Chen, N. Zhao, *Adv. Funct. Mater.,* 2014, **24**, 7102-7108
48 H.S. Kim, C.-R. Lee, J.-H. Im, K.B. Lee, T. Moehl, A. Marchioro, S.-J. Moon, R. Humphry-Baker, J.H. Yum, J.E. Moser, M. Grätzel, N.-G. Park, *Sci. Rep.* 2012**,** **2***,* DOI:10.1038/srep00591.
49 G. Niu, X. Guo, L. Wang, *Journal of Materials Chemistry A*, 2015, **3**, 8970-8980
50 R. Dong, Y. Fang, J. Chae, Z. Xiao, Q. Dong, Y. Yongbo, A. Centrone, X.C. Zeng, J. Huang, *Advanced Materials*, 2015, **27**, 1912

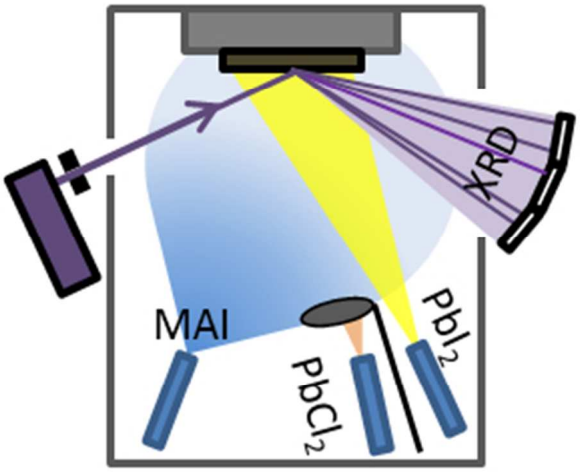

Graphical abstract